Surface waves propagating on a turbulent flow

Pablo Gutiérrez[1,2] and Sébastien Aumaître[1,3,a)]

[1]*Service de Physique de l'Etat Condensé, DSM, CEA-Saclay, CNRS URA 2464,*
91191 Gif-sur-Yvette, France
[2]*Departamento de Física, Facultad de Ciencias Físicas y Matemáticas,*
Universidad del Chile, Avenida Blanco Encalada 2008, Santiago, Chile
[3]*Laboratoire de Physique, ENS de Lyon, UMR-CNRS 5672, 46 allée d'Italie,*
F69007 Lyon, France

We study the propagation of monochromatic surface waves on a turbulent flow of liquid metal, when the waves are much less energetic than the background flow. Electromagnetic forcing drives quasi-two-dimensional turbulence with strong vertical vorticity. To isolate the surface-wave field, we remove the surface deformation induced by the background turbulent flow using coherent-phase averaging at the wave frequency. We observe a significant increase in wavelength, when the latter is smaller than the forcing length scale. This phenomenon has not been reported before and can be explained by multiple random wave deflections induced by the turbulent velocity gradients. The shift in wavelength thus provides an estimate of the fluctuations in deflection angle. Local measurements of the wave frequency far from the wavemaker do not reveal such systematic behavior, although a small shift is visible. Finally, we quantify the damping enhancement induced by the turbulent flow and compare it to the existing theoretical predictions. Most of them suggest that the damping increases as the square of the Froude number, whereas our experimental data show a linear increase with the Froude number. We interpret this linear relationship as a balance between the time for a wave to cross a turbulent structure and the turbulent mixing time. The larger the ratio of these two times, the more energy is extracted from the wave. We conclude with possible mechanisms for energy exchange. © *2016 AIP Publishing LLC.* [http://dx.doi.org/10.1063/1.4941425]

I. INTRODUCTION

Wave propagation through random media is the subject of intense studies,[1,2] owing to its ability to probe the properties of complex matter. Here, we consider surface waves propagating on a turbulent flow. These waves are both dispersive and nonlinear (see Equation (1)). They can be scattered by the velocity gradients and exchange energy with the underlying flow. Quantifying such energy exchange is a key issue in the context of ocean-atmosphere interactions, as well as for coastal swell forecasting. Indeed, the interactions between wind-generated gravity waves and the underlying turbulent flow are not fully understood, and they motivate many theoretical studies and *in situ* measurements in physical oceanography (see some examples in Refs. 3–7).

The scattering of monochromatic waves by a single vortex has been studied both experimentally and theoretically,[7–9] and some similarities with the Aharonov-Bohm effect have been underlined. Scaling laws have been proposed for turbulence-induced wave-damping.[10,11,13–15]

Lighthill[10] studied theoretically the elastic scattering of a sound wave by a turbulent flow. Phillips[11] considered the same problem for gravity waves. He developed a scaling theory for the wavelength λ, when it is smaller than the characteristic length L of the turbulent forcing. Fabrikant and Raevsky computed the cross section of a single vortex and applied it to gravity waves propagating

---

a)Author to whom correspondence should be addressed. Electronic mail: sebastien.aumaitre@cea.fr

28, 025107-1

on a turbulent drift flow.[12] Teixeira and Belcher[13] and Kantha[14] considered the energy exchanges due to wave-induced vortex-stretching, focusing on gravity waves of wavelength larger than L. Although both rely on different physical mechanisms, the point of view of Phillips, Fabrikant and Raevsky on one hand and the one of Teixeira and Belcher on the other lead to the same scaling law (see Section IV A). Indeed, both approaches suggest an increase in turbulent damping that is proportional to the square of Froude number, Fr, defined as the ratio of the flow velocity over the wave speed. Boyev[15] considered a more energetic underlying flow and proposed a different scaling law, where the turbulent damping is linear in Fr. Numerical studies are difficult, because they combine the challenges of high-Reynolds-number flow simulations with those of fluid-interface simulations. Guo and Shen devoted a laudable effort to solve these issues,[16,17] but up to now only a small range of parameters has been explored.[17]

There are previous experimental studies on surface waves interacting with a turbulent flow. Falcón and Fauve[18] studied the delayed onset of the Faraday instability in the presence of a chaotic electromagnetically forced underlying flow. They also exhibited modifications of the waves' statistical properties. Green *et al.*[19] considered a progressive wave on a flow generated by a vibrating grid. They suggest that turbulent dissipative decay rate is proportional to the square of the wave amplitude.

Using a similar device, Olmez and Milgram[20] suggested that the temporal damping due to turbulence is directly proportional to the turbulent mixing rate. They used arguments similar to those presented in Ref. 15. However, this result was not confirmed by Ermakov *et al.*[21] Using the threshold of the Faraday instability to determine the damping induced by a flow generated by a vibrating grid, these authors report a damping rate that agrees with Ref. 13. Note that oscillating grids introduce another frequency that can interfere with the one of the waves. Moreover, because they rely mainly on local probes, these experiments cannot study modifications of the wavelength. Finally, the action of spatiotemporal noise on the Faraday instability is by itself a complex noise-induced phenomenon.

Our experimental device combines the electromagnetic driving used in Ref. 18 to stir the flow and progressive waves generated by a paddle. The fluid is a liquid alloy, Gallinstan,[22] which has large electrical conductivity. This allows us to produce a strong Electromagnetic Driven Flow (EMDF) with negligible heating by Joule effect. This EMDF has rapid random fluctuations in the bulk of the fluid. Another advantage of Gallinstan over water is its lower kinematic viscosity (2.5 times smaller than water): the surface waves are less damped in Gallinstan than in water. The turbulent energy of the EMDF is large compared to the energy carried by the waves. Finally, using the diffusion of a laser sheet on the surface and triangulation techniques, we are able to track the surface elevation along a line in the direction of the wave propagation. The random fluctuations of the surface are removed by a coherent average procedure. We can therefore measure the wavelength of the propagating wave with and without EMDF, as well as the damping induced by turbulence.

In Section II, we present the main features of the experiment. The setup is described and some estimates of relevant dimensionless parameters are given. The main features of the EMDF and of the waves are described. In Section III, we focus on the increase in wavelength induced by the turbulent flow, when the wave frequency is large. It is understood in terms of random fluctuations of the direction of wave propagation. Section IV focuses on the enhancement of damping by the background turbulence. To interpret the data, we review some theoretical scalings, mainly based on dimensional arguments, and we confront them to our experimental findings. Our data suggest a linear scaling of the damping rate with Fr. This scaling may be interpreted as a balance between the time for a wave to cross a turbulent structure and the turbulent mixing time. The physical damping mechanism, as well as further studies, is discussed in Sec. V.

II. EXPERIMENTAL FEATURES

A. The setup

1. Turbulent flow and wave generation

The device driving the turbulent flow has been previously described in Ref. 23. It is depicted in Figure 1. It consists of a rectangular tank of size $0.5 \times 0.4 \times 0.1$ m³. It is filled with a layer of depth
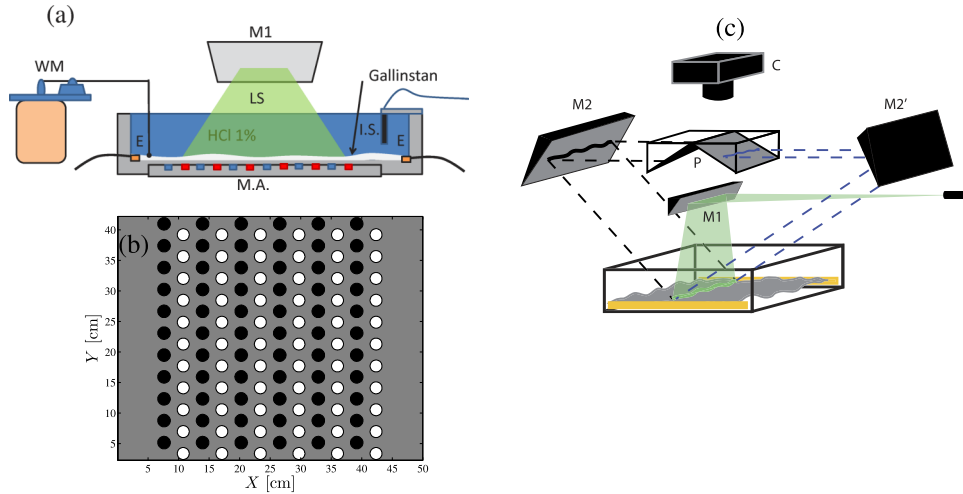
FIG. 1. Experimental device. (a) A cut along the wave propagation axis, with WM the Wavemaker, LS the Laser Sheet, MA the Magnet Array, IS the Inductive Sensor, and E the Electrodes. (b) The structure of the array of magnets beneath the cell. (c) Geometry of the device to track the diffused line. The laser sheet is shined towards the surface with the mirror M1. The diffused line is imaged twice on the camera C, with two opposite angles by the mirrors M2 and M2′. Each image is recorded on half of the camera sensor thanks to two prisms P.

$H = 1$ cm of Gallinstan covered by a layer of water slightly acidified to prevent the oxidation of the Gallinstan surface. The water layer is thick enough (about 8 cm) to make the water–Gallinstan interface insensitive to the boundary condition at top of the water layer (covered by a Plexiglas plate). Therefore, we study the deformation of a Gallinstan-water interface, Gallinstan being 6.5 times denser than water.

The Lorentz force stirs the fluid. It is generated by horizontal electrical current and an array of permanent disk-shaped magnets of opposite polarities, depicted in Figure 1(b). The distance between magnets defines the forcing length scale $l = 3.7$ cm. The magnetic field generated at the center of a magnet reaches $B = 0.12$ T at the bottom of the liquid metal layer, but it is reduced to 0.033 T at the liquid metal surface. The supplied current I ranges between 0 and 180 A, for most of the experiments presented here. I is the parameter controlling the velocity gradients and the turbulent strength, via the Lorentz force.

The waves are excited by a cylindrical paddle of length 100 mm and diameter 8 mm around a horizontal axis, in contact with the interface (see Figure 1). An electromagnetic shaker LDS 406 moves it vertically. In order to prevent strong nonlinearities and wave-breaking, the paddle displacement is limited at most to 10% of the wavelength. Hence, it never exceeds 6 mm for the longest generated wavelength. By pushing the fluid surface up and down, the paddle creates propagating waves without generating additional stream. The direction of propagation defines the x-axis. It is parallel to the applied electrical current. We drive the waves at frequencies ν between 3 and 9 Hz. The dispersion relation for the waves between two fluids is given by

$$\omega^2 = \left(\frac{\rho - \rho'}{\rho + \rho'}gk + \frac{\sigma}{\rho + \rho'}k^3\right)\tanh(kH), \tag{1}$$

where $k = 2\pi/\lambda$ is the wavenumber, $\omega = 2\pi\nu$ is the corresponding angular frequency, H is the fluid depth, g is the acceleration of gravity, σ is surface tension, ρ is the density of Gallinstan, and ρ' the density of acidified-water. The phase velocity $C_w = \omega/k$ and the group velocity $C_g = d\omega/dk$ differ in general. The limit of *deep water* is reached for $H/\lambda > 1$, hence $\tanh(kH) \sim 1$. The right-hand side of relation (1) reduces to a polynomial in this case. Capillarity dominates for $k \gg 1/l_c$ with $l_c = \sqrt{\sigma/(\rho g)} = 2.8$ mm the capillary length. Gravity is the main restoring force for $k \ll /l_c$. In deep water, when only one of the restoring forces dominates, dispersion relation (1) reduces to a power law. Unfortunately, Table I shows that we are in none of these two limits. Therefore, we have to use full dispersion relation (1) to compute C_w or C_g. Note that C_g is nearly constant,

TABLE I. Main features of the excited wave. The characteristic velocity of the flow U_o is estimated for a typical applied current of 160 A.

ν [Hz]	3	4	5	6	7	8	9
λ [cm]	8.48	6.15	4.74	3.83	3.21	2.76	2.44
$\tanh(kH)$	0.63	0.77	0.87	0.93	0.96	0.98	0.99
C_w [m/s]	0.25	0.25	0.24	0.23	0.22	0.22	0.22
C_g [m/s]	0.23	0.21	0.20	0.20	0.20	0.20	0.21
C_w/C_g	1.09	1.14	1.17	1.17	1.14	1.09	1.04
$Fr_w^{max} = U_o/C_w$	0.65	0.68	0.70	0.72	0.74	0.75	0.76
$Fr_g^{max} = U_o/C_g$	0.71	0.77	0.82	0.84	0.84	0.82	0.79

because our range of forcing frequencies is around its minimum (reached at 6.37 Hz). The surface tension between Gallinstan and water is not reported and has to be estimated. Moreover, it might depend on the acid concentration (about 1% in our experiment). By using the Faraday instability, we determined a surface tension of 0.5 N/m under our experimental conditions. The dispersion relation represented by the solid line in Figure 2 is obtained for this value of σ. We use mainly this value hereafter. However, the surface tension is very sensitive to the presence of impurities. As a consequence, we adjust it in some experiments to take into account the aging of the interface that explains the scattering of the experimental data in Figure 2. The correction never exceeds 20% of the nominal value (0.5 N/m).

2. Measurement techniques and averaging procedure

We use inductive sensors to measure the position of the wavemaker and to probe the surface locally. The technique to measure the elevation along the direction of propagation is sketched in Figure 1(c): A laser sheet is shined vertically onto the surface. The deformation of the line diffused by the surface gives access to the surface elevation, thanks to a triangulation method. The diffusion of the laser light is quite dim because of the high reflectivity of the Gallinstan surface. High sensitivity is therefore needed. However, the surface deformation may occasionally induce direct reflections towards the camera, which hide the diffused line. Therefore, two simultaneous pictures at different angles are required to follow the elevation of the entire line at all time. Indeed, the diffused line cannot be blinded at the same time and at the same position on both images. Instead of using two cameras, we built the optical setup shown in Figure 1, right. It allows us to gather two simultaneous pictures at angles of $\pm 37°$ with the vertical with the use of a single sensitive camera. An algorithm tracks the diffused line, which is assumed continuous and differentiable.
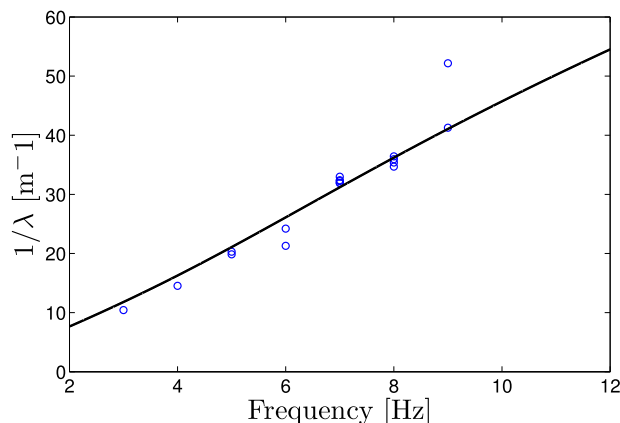

FIG. 2. Dispersion relation without turbulent flow. Circles correspond to experimental measurements. The full line is the prediction of Equation (1) with $\sigma = 0.5$ N/m.

To remove all the turbulent deformations that are not in phase with the wave, we perform a coherent phase average as suggested in Ref. 27. To do so, we take precisely n images per wave period ($5 \leq n \leq 15$). We perform an average over more than 100 periods of all detected lines that are exactly locked in phase with the excited wave. We therefore obtain n averaged profiles for various strengths of the turbulent EMDF. We reach a precision of 0.25 mm for the wavelength and 0.15 mm for the wave amplitude.

B. Dimensionless parameters

The Navier–Stokes equation driven by the Lorentz force exhibits a natural velocity scale $U_o = \sqrt{JBl/\rho}$, which corresponds to a balance between the advection term and the Lorentz force. Here, we use the forcing length l as the characteristic length of the flow. Thus, one gets the Reynolds number $Re = \sqrt{JB/\rho} \cdot l^{3/2}/\nu_G$, with ν_G the dynamic viscosity of Gallinstan. Taking the maximum value of the magnetic field $B = 0.12$ T, we can expect $U_o \sim 16$ cm/s for $I = 180$ A, and thus $Re = 1.5 \times 10^4$, in our device. These estimates are compared to experimental measurements in Sec. II C. Note that the Reynolds number Re achieved here is 10 times larger than the one of grid generated flows.[19–21] Such estimates of the Reynolds number give a Kolmogorov length, $l_K = \rho \eta^{3/4}/\epsilon^{1/4} \sim 3 \times 10^{-2}$ mm with $\epsilon \sim U_o^3/L$ the energy flux per unit mass. In a thin fluid layer, the friction on the bottom induces extra damping of the velocity field. This friction term acts at all scales and modifies the scalings of two-dimensional (2D) turbulence.[24] In a liquid metal subject to electromagnetic forcing, friction is concentrated in a thin magnetic boundary layer where the electromagnetic induction phenomena focus the electrical currents and the velocity gradients.[25] The depth of this layer $e_H = H/Ha$ is characterized by the Hartmann number $Ha = \sqrt{\sigma/\eta}BH$.[22] e_H can be as small as 0.2 mm just above the magnets. One can evaluate this friction strength from the Reynolds number built on Hartmann-layer thickness, $Re_H = Re_L/Ha \cdot H/L = \sqrt{JlR/\sigma\nu B} \sim 100$. Therefore, the system generates a highly anisotropic nonlinear flow with mainly vertical vorticity.

A key dimensionless parameter in the study of the wave-mean-flow interactions is the ratio of the flow velocity over the wave velocity. For acoustic nondispersive waves, it defines the Mach number. For dispersive surface waves, it is called the Froude number. One can distinguish between the Froude number based on the phase velocity of the wave $Fr_w = U_o/C_w$ and the one based on the group velocity of the waves $Fr_g = U_o/C_g$. Note that the Froude numbers introduced here are built using the full gravito-capillary wave velocity (i.e., including capillary effects). As mentioned previously, Table I shows that none of these two effects is negligible in our experiment. The Froude number based on the root mean square (RMS) velocity is smaller by a factor of approximately 0.4 than the one shown in Table I. Nevertheless, we achieve larger Froude numbers than previous experiments.[18–21] Furthermore, the energy per unit volume contained in the turbulent flow, $E_t = \rho \langle U^2 \rangle$, is much larger than the energy of the generated wave, $E_w = \rho h_o^2 \omega^2$, with h_o the wave amplitude. The ratio between these energies can be expressed as $E_t/E_w = (Fr_w \cdot \lambda/h_o)^2$. Here, we keep the wave steepness h_o/λ less than 0.1 to prevent wave breaking. Therefore, the energy ratio is larger than 10 in most of our parameter range. One then expects stronger interaction and new interesting effects of the flow on the waves.

C. General features of the EMDF

We first characterize the EMDF, which is detailed in Ref. 22. To estimate the velocity field without waves, we seed the surface with millimetric particles of density $\rho_p = 2000$ kg/m^3. The particles are lighter than Gallinstan ($\rho_p/\rho \sim 0.3$),[21] and heavier than water ($\rho_p/\rho' \sim 2$), and are therefore floating on the Gallinstan-water interface. Using standard particle-tracking velocimetry, we measure the horizontal velocity of these floaters. In Figure 3, the RMS velocity of the floaters is compared to U_o, showing a linear relation, as expected. U_o overestimates the RMS velocity because it is computed with the maximum magnetic field. Note that the linear fit does not pass through zero, because the linear scaling in U_o does not hold at low velocity, where viscous effects dominate
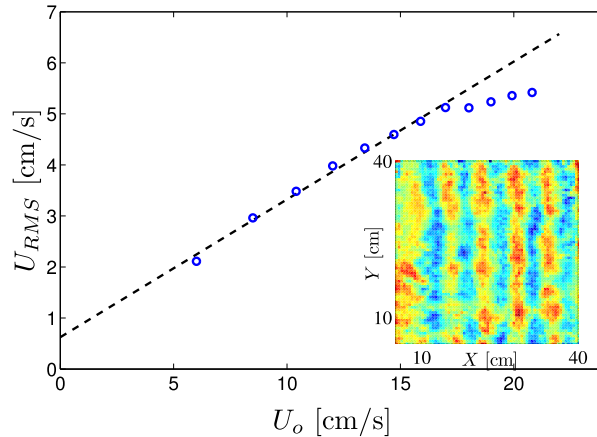
FIG. 3. Main panel: RMS velocity of floaters tracked at the liquid metal surface, U_{RMS}, as a function of the characteristic magneto-hydrodynamic velocity $U_o = \sqrt{JBl/\rho}$. The slope of the linear fit (dashed line) is 0.27. Inset: spatial distribution of vertical vorticity averaged over 60 s, for a driving current of I = 150 A (U_o=14.7 cm/s). The color map extends from -10 s^{-1} (blue) to 10 s^{-1} (red).

over nonlinearities. A small departure from linearity is also observed at high current. It may be the consequence of intense vertical motion taking place for strong driving, both at the surface and in the bulk of the flow. Our horizontal measurement cannot take this motion into account, resulting in a mismatch between the energy input by the electromagnetic forcing and the one estimated from the measurement. 2D turbulence exhibits an inverse cascade, concentrating the energy at the largest scale allowed by the setup. This does not seem to occur in our flow, which is neither fully turbulent nor fully 2D. In contrast, the average vertical vorticity (estimated from floaters motion[22]) exhibits structures of the size comparable to the width of the magnet stripes, as shown in the inset of Figure 3. The forcing length scale l therefore seems to be the relevant one to characterize the turbulent flow. The mean flow contains only a fraction (30%) of the total kinetic energy of the flow. One can see the EMDF as a strongly fluctuating flow where vertical vortices of size l compete with each other and interact in an unpredictable way. These vertical vortices induce significant depletion of the surface. At the highest Froude number, they can even radiate surface waves. The fluctuations of the surface elevation have a standard deviation around 0.5 mm for $I = 200$ A, and they are not Gaussian. It is therefore very important to perform a coherent phase average to remove all these incoherent fluctuations induced by the EMDF, in order to properly focus on the waves.

D. General features of the propagating wave

Figure 4 gives an example of the surface deformation induced by the waves after performing a coherent phase average. The n averaged curves sampled during a period are represented, for a wavemaker exciting waves at 8 Hz. We can always distinguish at least one wave oscillation with a clear wavelength near the wavemaker (chosen as origin of the coordinates). As the wave propagates, damping is visible: the wave propagates on a shorter distance when the supplied current (and therefore the turbulence strength) is increased: additional damping originates from the turbulent flow. Figure 5 shows the Power spectral density (PSD) of the deformation plotted in Figure 4. A close look around the main wavenumber peak reveals a shift of the wavelength that cannot be seen directly on the averaged profiles. Indeed the abscissa of the PSD maximum (approximated by a polynomial fit) shifts to smaller values when the turbulent intensity increases. This implies that the wavelength increases with the turbulence strength. In Sec. III, we study this wavelength shift and we try to detect possible frequency shifts and in Sec. IV, we quantify the turbulent enhancement of damping. These studies are performed for various excitation frequencies and amplitudes of the waves, together with various strengths of the turbulent flow.
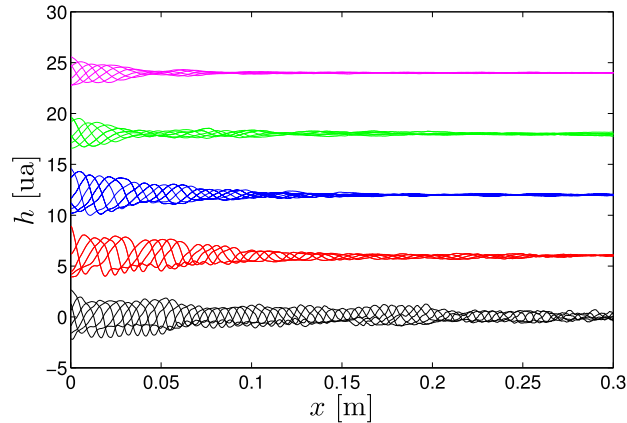
FIG. 4. Spatial profiles of the surface elevation after coherent phase averaging. The forcing frequency is 8 Hz and the forcing amplitude $h_o = 1.13$ mm (without turbulence). The currents driving the turbulent flows are $I = 0$ A (black), $I = 40$ A (red), $I = 80$ A (blue), $I = 120$ A (green), and $I = 160$ A (magenta). For each I a vertical displacement has been introduced for clarity.

III. WAVELENGTH AND FREQUENCY SHIFTS

A. Shift in wavelength

In order to study the shift in wavelength for all the EMDFs and all the excitation frequencies of the wave, we also compute the wavelength of the first oscillations of the profile (actually, twice the average length of the first four half-periods). Indeed, for strong turbulent damping, the oscillating part of the profile is quickly damped. For low excitation frequency, only a few periods remain, and the study of the PSD peaks does not yield an accurate determination of the wavelength. We checked that both signal processing methods lead to the same wavenumber at large excitation frequency. The main panel of Figure 6 shows this effective wavelength as a function of *Fr* measured for various excitation frequencies of the wave. In Figure 6, the increase in wavelength occurs for excitation frequencies larger than 5 Hz. Below 5 Hz the wavelength is nearly constant in our range of Froude number. We have not noticed any significant modification when changing the amplitude of the waves, h_o, in the range of forcing tested in our experiment. Hence, the shift seems insensitive to the waves nonlinearity (quantified by the steepness h_o/λ).

We wish to explain the increase in wavelength at high excitation frequency. To wit, one must recall that the wave is advected by the underlying turbulent velocity field. Hence, for $\lambda_o \ll l$, with
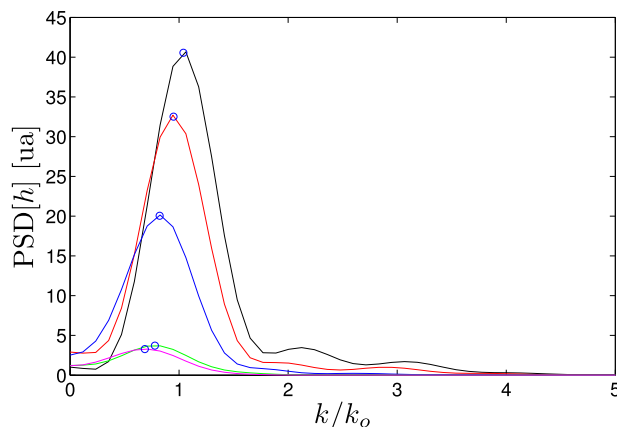

FIG. 5. Power Spectrum Density (PSD) of the elevation profiles of Figure 4. The circles show the peak value determined through polynomial fitting.
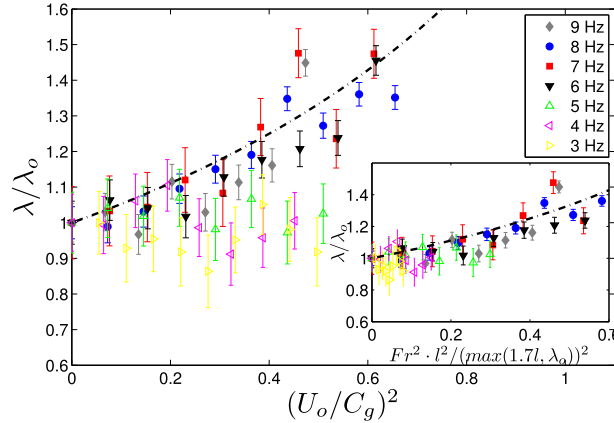
FIG. 6. Shift in wavelength induced by the turbulent flow at various excitation frequencies. The dotted-dashed line corresponds to the relation $\frac{\langle \lambda \rangle}{\lambda_o} = \frac{1}{1-Fr^2}$ (see Equation (2)). In the inset, the x-axis of the lowest excitation frequency (below 5 Hz, i.e., $\lambda_o \geq 1.7l$) is weighted by l/λ_o.

λ_o the forced wavelength, the wave does not propagate in a straight direction. However, we measure experimentally k_x, the projection of the wave vector of this deflected wave on the x-axis. We assume that the shift in wavelength traces the fluctuations in the direction of propagation. Indeed, let us denote as θ the small angle between the wavevector and the x-axis. For small θ, this deviation induces a component of the wavevector $k_y/k_o = \sin(\theta) \sim \theta$ and $k_x/k_o = \cos(\theta) \sim 1 - \theta^2/2$, where k_o is the wavevector's modulus and k_x, k_y are its projections on the x-axis and the y-axis, respectively. The rotation of the wavevector is due to the flow gradients. The wave packet crosses a flow structure of size l_i during a time l_i/C_g, where the index i labels each structure of the flow. During this time, the wave crest is displaced by approximately $\Delta y_i = \Delta U_i \cdot l_i/C_g$ where ΔU_i is the velocity increment induced by the structure i. For $\lambda_o \ll l$, the deflection of the wave is given by $\theta_i = \Delta y_i/l_i$. On average there is no mean flow; hence $\langle \Delta k_y \rangle = 0$, but $\langle U_i^2 \rangle \propto U_o^2$ and

$$\frac{\langle k_x \rangle}{k_o} = 1 - \frac{Fr_g^2}{2}. \tag{2}$$

The dashed line shows this scaling-law in Figure 6. It agrees with the higher excitation frequencies. In this limit, the shift in wavelength seems to originate from fluctuations of the deflection angle of the wave, $\langle \theta^2 \rangle$, induced by the flow.

In the opposite limit $\lambda_o > l$, Figure 6 shows that the wavelength is constant. Therefore, the underlying flow does not deviate the wave anymore. A sharp transition between these two regimes appears in Figure 6 for λ_o/l between 1.7 and 1.4. Note that in the limit $\lambda_o \gg l$, one may prefer to express the deflection as $\theta_i = \Delta y_i/\lambda_o = (\Delta U_i \cdot l/C_g) \cdot (\nu_f/C_w)$ where ν_f is the forcing frequency. Therefore, one expects $\langle k_x \rangle/k_o = 1 - (Fr_g \cdot l \cdot \nu_f/C_w)^2/2$ for $\lambda_o \gg l$. If we assume $\theta_i = \Delta y_i/\lambda_o$ for $\lambda_o > 1.7l$ and $\theta_i = \Delta y_i/l$ for $\lambda_o < 1.7l$, then the inset of Figure 6 shows that all curves collapse together. All the points at large wavelength are sent near the origin because the control parameter of the deflection is $Fr_g \cdot l/\lambda_o$ in this limit. This parameter remains small (less than 1/3) in the considered cases.

B. Frequency shift

The shift in wavenumber naturally raises the question of a possible frequency shift for a wave propagating through the randomly moving medium. At small Froude number, and in the limit of a small wavelength compared to the distance between scatterers, we expect a frequency shift weaker than the wavenumber one. Indeed, in this limit, relation (17) from Ref. 26 implies a Doppler shift of the frequency satisfying $\Delta \omega/\omega_o \sim (C_g/C_w) \cdot (\Delta k/k_o)Fr$ where $\Delta \omega$ and Δk are the frequency and wavenumber shifts at a given point and at a given time. Hence, the normalized frequency shift is
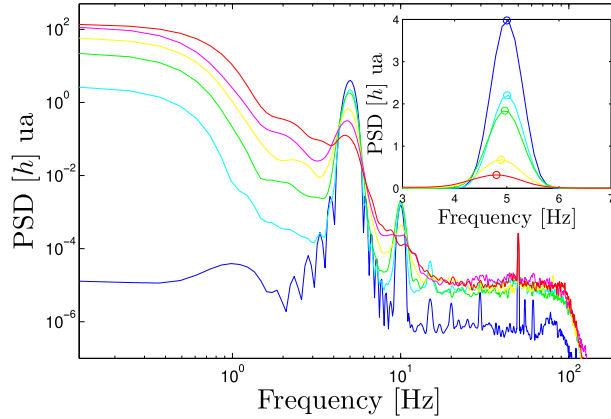
FIG. 7. PSD of the local fluctuations in time of the surface elevation for a forcing frequency of 5 Hz. The forcing intensities are $I = 0$ A (blue), $I = 20$ A (cyan), $I = 40$ A (green), $I = 60$ A (yellow), $I = 80$ A (magenta), and $I = 100$ A (red). The inset displays a zoom of the PSD of the elevation, band-pass filtered around the forcing frequency.

reduced by a factor of the order of the Froude number, as compared to the wavenumber shift. For a random velocity field with zero mean, one might have to push the expansion to higher order. Moreover, as we excite the waves at a constant rate, one may expect that the frequency should be fixed close to the paddle.

To detect a possible frequency shift induced by the turbulent flow, we have placed an inductive sensor 36 cm away from the paddle and 12 cm away from the propagation axis. Note that such a sensor has a good resolution in the vertical direction but not in the horizontal ones: it filters out the small wavelengths. In addition, fluctuations of the surface elevation induced by the turbulent motion cannot be eliminated through coherent averaging. Consequently, the measurements at low frequencies might be perturbed by the turbulent background and the measurements at large frequencies might be biased by the sensor cutoff.

The PSD of the local fluctuations in time of the surface elevation is shown in Figure 7 for a forcing frequency of 5 Hz. Despite the increase of the power spectrum at low frequency, a peak can be seen until $I = 80$ A. The bump at low frequency, which increases with the driving, is due to the slow motion of the surface depletions induced by the motion of competing vortices. A closer look at the remaining peak around the excitation frequency reveals a shift. It is underlined in the PSD of the band-pass filtered signal, presented in the inset of Figure 7. This shift is shown in Figure 8
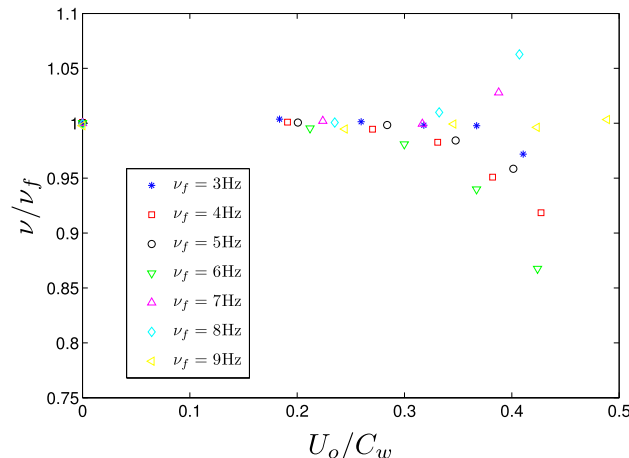

FIG. 8. Frequency shift as a function of the Froude number (based on the phase velocity of the waves). Each symbol corresponds to one forcing frequency.

for various Froude numbers and various excitation frequencies. Unlike the wavelength shift, the sign of the frequency shift seems to depend on the excitation frequency ν_f. Two regimes can be identified, separated by $\nu_f = 6$ Hz. Below this value, the measured frequency decreases with the Froude number. Above $\nu_f = 6$ Hz, it seems to be nearly constant or even to increase. The shift never exceeds 15% and is weaker than the wavenumber shift, as expected. We should stress the fact that this shift must depend on the distance travelled by the wave through the turbulent medium and on the local properties of the flow. Hence, the shift could evolve with the sensor position. This makes difficult a quantitative comparison between the locally measured frequency shift and the wavenumber shift evaluated over the whole length of the contained. A systematic study of the wavenumber and frequency as a function of space would require a much larger device, in order to define unambiguously a local wavelength and a local frequency. This interesting extension of our study is, however, beyond the scope of the present work.

IV. TURBULENT DAMPING

A. Theoretical predictions

We now focus on the spatial damping of the profiles obtained by coherent averaging and displayed in Figure 4. Recall that the coherent average is obtained by locking the acquisition of the surface profiles with the excitation frequency. The enhancement of the damping is attributed here to the increase in turbulent fluctuations. Theoretically, enhanced damping may have two origins: it could be due to scattering of the wave in various directions by velocity gradients, or it could be induced by energy exchanges with the underlying flow. In this section, we first review the corresponding theoretical predictions and recall their ranges of validity. The assumptions of the various theoretical models never quite fit our experimental conditions. Nevertheless, we can check if some theoretical predictions agree with our data, in order to extend these ideas to our experimental conditions. When doing this comparison, we focus particularly on the scaling laws between the turbulent damping rate and the Froude number.

1. Elastic scattering

The damping of sound waves due to elastic scattering on turbulent structures has been considered in Ref. 10. For sound waves with a wavelength smaller than the Taylor microscale, λ_T, a damping rate $\gamma_{turb} \propto (\langle v^2 \rangle / c^2) / \lambda_T$ is suggested, with c the sound speed. Phillips used similar elastic scattering arguments to determine the damping of surface gravity waves by turbulence.[11] In the oceanographical context he considered, the wavelength of the gravity waves is smaller than the forcing length scale of the background turbulence. Moreover, he restricted his analysis to the *single scattering limit* and Born approximations. This limit is valid only when the scatterers are scarce. In this case, the complete wave field can be approximated by the incident wave in the scattering process. It requires a wave energy much larger than the turbulent energy. In terms of Froude number, one needs $Fr_w \ll h_o/\lambda$. This approach has been extended later to drift flow turbulence by Fabrikant and Raevsky.[12] In our experiment, we keep the wave steepness $h_o/\lambda < 0.1$ in order to prevent wave breaking. The second and less demanding requirement concerns the duration vorticity fluctuations. It must be small compared to the time spent by the wave inside the turbulent area. This corresponds to $l/L \ll Fr$. In our experimental cell, one has always $Fr > h_o/\lambda$. Hence, we are not in the single scattering limit. As a consequence, the predictions of Phillips, $\gamma_{turb}/k = (k \cdot l)^{-2/3} Fr^2$, may not be relevant to interpret our experimental results.

Note, however, that in Section III A we have interpreted the shift in wavelength as an elastic deflection of the wave by the flow, in the limit of small wavelength. We have established that the variance of the deflection angle is $\langle \theta^2 \rangle = Fr^2$. We can infer a *total scattering cross section* (actually a line in the case of surface waves) of the wave from this deflection: $\sigma* = a(1 - \langle \cos(\theta) \rangle) \sim a \cdot Fr^2$, where $a \leq l$ would be associated to the mean size of the vortex core. Therefore, we know formally the density of vortices $n \sim 1/l^2$, the mean free path of the wave $l^* = l^2/(a \cdot Fr^2) \leq l/Fr^2$, and the number of scattering events during the propagation through the entire cell, $N^* = L/l^* \leq Fr^2 \cdot L/l \approx 4$.

This shows that we are not in the multi-scattering regime in which the waves follow a diffusive random walk in the disordered medium. Hence, if the damping is mainly due to elastic scattering, we can approximate the damping coefficient by $1/l^*$ and hence $\gamma_{turb} \propto Fr^2 \cdot a/l$. Concerning the scaling in *Fr*, this crude estimate agrees with the Phillips, Fabrikant, and Raevsky predictions. Note however that these authors have shown that the scattering of surface gravity waves by a vortex is a complex phenomenon, and that the scattering cross section is far from being isotropic.[12]

2. Vortex stretching

More recently, Teixeira and Belcher studied the opposite limit, where the wavelength is larger than the integral scale of the turbulent flow.[13] They used the rapid distortion theory requiring $\lambda \gg l$ and $Fr \ll h_o/\lambda$. In this framework, they proposed a mechanism of energy transfer from the wave to the turbulence, via a stretching of vortices induced by the Stokes drift of the surface wave. They obtained $\gamma_{turb}/k = \langle \delta U_o^2 \rangle / C_g^2$.

One should notice that despite the different mechanisms and limits considered in Refs. 11 and 13, both approaches end up with the same kind of scaling law. Therefore, the scaling in Froude number is not sufficient to infer the underlying physical mechanism. Indeed, Phillips found a damping

$$\gamma_{turb} \propto \frac{k^2}{C_g^2} \int_{-\pi}^{\pi} \Phi(\kappa) d\theta, \tag{3}$$

where κ is the scattered wavevector, θ the scattered angle, and $\Phi(\kappa)$ is the power spectrum of the vertical vorticity. Dimensionally, it implies a damping $\gamma_{turb} = k \langle \delta v_k^2 \rangle / C_g^2$, where $\delta v_k = U_o(l \cdot k)^{-1/3}$ is the typical turbulent velocity increment on a scale k. In the single scattering limit, the velocity increments on a scale of order of the wavelength are the most involved in the damping process. Teixeira and Belcher exhibited a damping process of the wave energy, E_w, involving turbulent Reynolds stresses (proportional to U_o^2) times the velocity gradient of the Stokes drift (proportional to $h_o^2 k^2 \omega$). One gets $\frac{1}{E_w} \frac{dE_w}{dt} \sim \frac{U_o^2 \cdot (h_o^2 k^2 \omega)}{(h_o \omega)^2}$ and $\gamma_{turb} \propto \frac{1}{C_g \cdot E_w} \frac{dE_w}{dt} \sim k(U_o/C_g)^2$. Therefore, both approaches scale with the square of the Froude number. They only differ in their dependence on wavenumber, because they involve a different amount of turbulent kinetic energy. Unfortunately, as in most table-top experiments, we are in the crossover region where the wavelengths are of the order of the forcing scale. Moreover, the requirement that $Fr \ll h_o/\lambda$, shared by the two models, is not satisfied by our setup.

3. Turbulent advection

Boyev considered the case where the energy of the turbulent flow is much larger than the energy carried by the wave. It is a relevant assumption for our experiment. He also assumed that the turbulent time scale is much smaller than the wave period, to facilitate efficient mixing of the energy.[15] The former assumption imposes $h_o/\lambda \ll Fr$, which is nearly true in our experiment. The latter assumption implies $l/\lambda \ll Fr$ which is clearly not satisfied in our device. In the deep-water model proposed by Boyev, the energy in the wave is limited to a shallow layer (of depth of order $1/k$). This energy of the wave is advected into the bulk flow at the turbulent mixing rate, Ω_m. Using the estimate of the mixing rate across a layer of size $1/k$ proposed in Ref. 20, $\Omega_m = U_o k^{2/3}/l^{1/3}$, one gets

$$\gamma_{turb} \propto \frac{U}{C_g(k)} k \cdot (l \cdot k)^{-1/3}. \tag{4}$$

This mechanism, which transfers energy from wave into the deep turbulence, is not efficient in our layer of Gallinstan, where the depth is small and where vorticity is mainly vertical. However, one can assume that a similar mechanism is at work: a horizontal mixing rate can scatter the waves and extract the energy from the direction of propagation.

B. Experimental results

There are many ways to characterize the damping from the profiles shown in Figure 4, and all should be equivalent. We choose to compute the standard deviation of the profile. Assuming an exponential turbulent decay with damping coefficient γ_{turb}, one has a *damping enhancement*: $\gamma_{turb}/\gamma_o \propto \sqrt{\langle \Delta h_o^2 \rangle}/\sqrt{\langle \Delta h_{turb}^2 \rangle}$, where Δh is the surface deformation induced by the wave and where the subscripts o and $turb$ correspond, respectively, to the cases without and with turbulence. Assuming that all viscous effects (including purely magnetic damping, as discussed below) are included into γ_o, one expects $\gamma_{turb}/\gamma_o \propto F(U/C_g, h_o/\lambda_o, k_o \cdot l, C_w/C_g)$. In our range of parameters, the ratio of the phase velocity over the group velocity does not evolve much (see Table I); hence, it can be excluded from the scaling law. For a given frequency, we note that a better collapse of the curve γ_{turb}/γ_o vs U/C_g is obtained if the damping enhancement is multiplied by the wave steepness h_o/λ_o. It also improves the data collapse at high frequency (above 6 Hz). The benefit is less obvious at lower frequencies. Note that the higher frequencies do not correspond necessarily to the higher steepness since we vary also the forcing amplitude. Moreover, we can also express the damping ratio γ_{turb}/γ_o as a function of the combination: $Fr_g \cdot l/\lambda_o$. Indeed, this parameter can be interpreted as the ratio of two characteristic time scales: (i) $\tau_w = l/C_g$, the time spent by the wave to cross a turbulent structure and (ii) $\tau_m = \lambda_o/U_o$, the horizontal turbulent mixing rate over a size λ_o. It can be thought of as the time used by the turbulent flow to move the fluid by about a wavelength.

Figure 9 shows the variations of the turbulent damping enhancement multiplied by the steepness as a function of the time ratio $\tau_w/\tau_m = Fr_g \cdot l/\lambda_o$ in logarithmic representation. We choose these parameters to stress the role of the two time scales τ_m and τ_w. The best fit is linear (dotted-dashed line), in agreement with the scaling proposed in Ref. 15. The dashed-line represents a scaling with power 2, which gives a bad fit. This linear behavior in terms of mixing rate promotes a damping mechanism by turbulent advection.[15,20] However, in our experimental configuration, it is most probable that the energy of the waves departs from its propagation direction because of *horizontal advection* by the vertical vorticity. The linear elastic scattering that can explain the wavelength shift would then involve the square of the Froude number. Hence, it is not the main mechanism implied in the damping. The action of the wave amplitude remains puzzling. It may trace the role of the nonlinearity (proportional to the steepness) as suggested in Ref. 19 or it may underline the Stoke drift of the wave (having a velocity proportional to $C_w(h_o/\lambda)^2$).

Finally, we have not yet considered pure magneto-hydrodynamic (MHD) effects regarding the damping. Without applied currents, it has been shown that the wave motion above a magnetic field induces Foucault currents that dissipate energy by Joule effect and hence damp the waves.[28] This
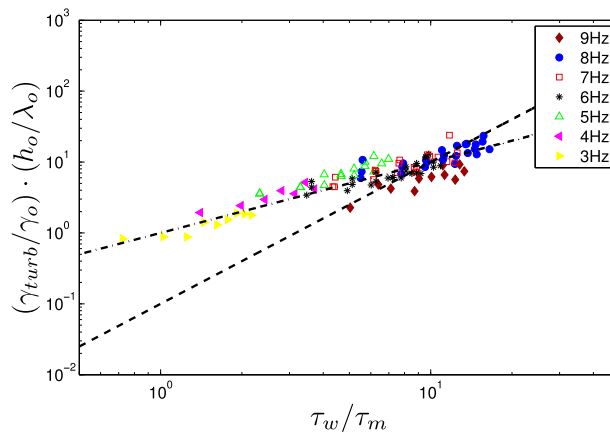

FIG. 9. Damping induced by the turbulent flow as a function of the ratio between the time spent by the wave to cross a turbulent structure, τ_w, and the turbulent mixing time over a length λ_o, τ_m, with $\tau_w/\tau_m = Fr_g \cdot l/\lambda_o$, for various excitation frequencies and amplitudes. The dashed line corresponds to $\gamma_{turb} \propto (U/C_g)^2$, and the dotted-dashed line corresponds to $\gamma_{turb} \propto (U/C_g)$.

effect is taken into account in γ_o. When an applied current is added, the full problem involves both surface deformation by the wave and the flow and induction of an inhomogeneous magnetic field. It is difficult to make predictions in this very complex configuration. One may assume that the wave modulates the EMDF by modulating the Hartmann layer for instance. This might induce resonances when the wavelength matches the meshsize of the array of magnets. Hence, MHD effects cannot be ruled out, as far as the role of the amplitude in the damping enhancement is concerned. This would deserve further theoretical studies.

V. DISCUSSIONS AND CONCLUSIONS

We have reported an experimental study of a wave propagating on an almost 2D flow. Our experimental setup has a large ratio of turbulent energy to wave energy. We observe a significant shift in the component of the wavenumber along the direction of propagation, as long as the excited wavelength is smaller than the forcing length scale of the turbulent flow. In this case, the projection of the wavevector along the main propagation axis decreases when the Froude number increases. To our knowledge, this has not been reported before. This shift is interpreted as the signature of the fluctuations of the direction of wave propagation. Our argument assumes that the modulus of the wavevector is conserved during the wave propagation on the turbulent flow. However, a shift in wave frequency is also observed far from the forcing point. These results raise the question of an effective dispersion relation for a surface wave on top of an underlying complex flow. Indeed, usual dispersion relation (1) is deduced only for a potential wave flow, without background turbulence. When there is such a background turbulent flow, the separation between a surface wave and a background flow is questionable. Some procedures are suggested in Ref. 27, but no modifications of the dispersion relation are proposed by these authors. Dispersion relations have been computed recently in some specific cases with vertical vorticity, and only along a single horizontal direction (1D-waves).[29,30] To go further in this direction, a complete characterization of the surface deformation in the frequency-wavenumber space would be useful. The wavemaker could be driven by a random excitation, in order to generate several frequencies and wavenumbers. However, we do not have accurate enough spatial and temporal resolutions to determine the full dispersion relation in the presence of randomly moving fluid. Another difficulty would be to accurately remove the deformation induced by the flow. Finally, at large Froude number, the flow may spontaneously generate waves.[31]

A second point of our study concerns wave damping. We show that turbulent damping increases with the Froude number. The best fit is linear with the Froude number, as proposed in Refs. 15 and 20. The observed enhancement of damping is incompatible with the quadratic scaling proposed by Phillips, Fabrikant and Raevsky and by Teixeira and Belcher.[11–13] The linear scaling can be interpreted as a consequence of horizontal mixing of the energy of the progressive waves. Two scenarios remain possible: (i) the energy is deviated but remains in the form of surface waves or (ii) it is mainly absorbed into the bulk turbulent flow. In the former case, the total energy of the surface wave field is conserved, although the energy can be transferred nonlinearly to other wavenumbers. In the second case, the energy is directly exchanged with the flow and the scattering of the waves is strongly inelastic. To discriminate between these two mechanisms, a 2D measurement of the entire surface deformation would be helpful. This is very challenging for a liquid metal surface. Nevertheless, one advantage of our device is that we can easily generate various types of flows. For instance, we force here mainly vertical vortices, but we could also generate horizontal vortices, with axes aligned with the wave crests. We expect a very different action of the flow in this case. This modification should help distinguish between damping due to elastic scattering and damping induced by advection of the wave energy. Finally, measuring the mean power injected by the wavemaker as function of the turbulence strength could give new insights into this question.

ACKNOWLEDGMENTS

[1] P. Sheng, *Introduction to Wave Scattering Localization and Mesoscopic Phenomena* (Academic Press, San Diego, CA, USA, 1995).

[2] A. Ishimara, *Wave Propagation and Scattering in Random Media* (IEEE Press, New York, NY, USA, 1997).

[3] O. M. Phillips, *Dynamics of the Upper Ocean*, 2nd ed. (Cambridge University Press, 1977).

[4] S. A. Kitaigorodskii, M. A. Donelan, J. L. Lumley, and E. A. Terray, "Wave-turbulence interactions in the upper ocean. II. Statistical characteristics of wave and turbulent components of the random velocity field in the marine surface layer," J. Phys. Oceanogr. **13**, 1988–1999 (1983).

[5] F. Ardhuin and A. D. Jenkins, "On the interaction of surface waves and upper ocean turbulence," J. Phys. Oceanogr. **36**, 551–557 (2006).

[6] F. Veron, W. K. Melville, and L. Lenain, "Measurements of ocean surface turbulence and wave–turbulence interactions," J. Phys. Oceanogr. **39**, 2310–2323 (2009).

[7] B. Gallet and W. R. Young, "Refraction of swell by surface currents," J. Mar. Res. **72**, 105–126 (2014).

[8] F. Vivanco and F. Melo, "Experimental study of surface waves scattering by a single vortex and a vortex dipole," Phys. Rev. E **69**, 026307 (2004).

[9] Ch. Coste, F. Lund, and M. Umeki, "Scattering of dislocated wave fronts by vertical vorticity and the Aharonov-Bohm effect. I. Shallow water," Phys. Rev. E **60**, 4908–4916 (1999); Ch. Coste and F. Lund, "Scattering of dislocated wave fronts by vertical vorticity and the Aharonov-Bohm effect. II. Dispersive waves," *ibid.* **60**, 4917–4925 (1999).

[10] M. J. Lighthill, "On the energy scattered from the interaction of turbulence with sound or shock waves," Proc. Cambridge Philos. Soc. **49**, 531–551 (1953).

[11] O. M. Phillips, "The scattering of gravity waves by turbulence," J. Fluid Mech. **5**, 177–192 (1959).

[12] A. L. Fabrikant and M. A. Raevsky, "Influence of drift flow turbulence on surface gravity wave propagation," J. Fluid Mech. **262**, 141–156 (1994).

[13] M. A. C. Teixeira and S. E. Belcher, "On the distortion of turbulence by a progressive surface wave," J. Fluid Mech. **458**, 229–267 (2002).

[14] L. Kantha, "A note on the decay rate of swell," Ocean Model. **11**, 167–173 (2006).

[15] A. G. Boyev, "The damping of surface waves by intense turbulence," Izv., Atmos. Ocean. Phys. **7**, 31–36 (1971).

[16] X. Guo and L. Shen, "Interaction of a deformable free surface with statistically steady homogeneous turbulence," J. Fluid Mech. **658**, 33–62 (2010).

[17] X. Guo and L. Shen, "Numerical study of the effect of surface wave on turbulence underneath. II. Eulerian and Lagrangian properties of turbulence kinetic energy," J. Fluid Mech. **744**, 250–272 (2014).

[18] C. Falcón and S. Fauve, "Wave-vortex interaction," Phys. Rev. E **80**, 056213 (2009).

[19] T. Green, H. Medwin, and J. E. Paquin, "Measurements of surface wave decay due to underwater turbulence," Nat. Phys. Sci. **237**, 115–117 (1972).

[20] H. S. Olmez and J. H. Milgram, "An experimental study of attenuation of short water waves by turbulence," J. Fluid Mech. **239**, 133–156 (1992).

[21] S. A. Ermakov, I. A. Kapustin, and O. V. Shomina, "Laboratory investigation of damping of gravity-capillary waves on the surface of turbulized liquid," Izv., Atmos. Ocean. Phys. **50**, 204–212 (2014).

[22] From the safety datasheet acc, Guideline 93/112/EC of Germatherm Medical AG, the Gallinstan is made of 68.5% of Gallium, 21.5% of indium, 10% of Tin, Its density is $\rho = 6.440 \times 10^3$ kg/m^3, its dynamic viscosity is $\nu_G = 3.73 \times 10^{-7}$ m^2/s, its electrical conductivity $\sigma = 3.46 \times 10^6$ S/m.

[23] P. Gutierrez, "Effects on the free surface of a turbulent flow," Ph.D. thesis, Ecole Polytechnique, 2013.

[24] Y. K. Tsang and W. R. Young, "Forced-dissipative two-dimensional turbulence: A scaling regime controlled by drag," Phys. Rev. E **79**, 045308(R) (2009).

[25] J. Sommeria, "Experimental study of the two-dimensional inverse energy cascade in a square box," J. Fluid Mech. **170**, 139–168 (1986).

[26] D. Censor, "The group doppler effect," J. Franklin Inst. **299**, 333–338 (1975).

[27] S. A. Kitaigorodskii and J. L. Lumley, "Wave-turbulence interactions in the upper ocean. I. The energy balance of the interacting fields of surface wind waves and wind-induced three-dimensional turbulence," J. Phys. Oceanogr. **13**, 1977–1987 (1983).

[28] B. Seernivasan, P. A. Davidson, and J. Etay, "On the control of surface waves by a vertical magnetic field," Phys. Fluids **17**, 117101 (2005).

[29] A. Constantin, "Dispersion relations for periodic traveling water waves in flows with discontinuous vorticity," Commun. Pure Appl. Anal. **11**, 1397–1406 (2012).

[30] C. I. Martin, "Dispersion relations for periodic water waves with surface tension and discontinuous vorticity," Disc. Contin. Dyn. Syst. **34**, 3109–3123 (2014).

[31] R. Savelsberg and W. van de Water, "Turbulence of a free surface," Phys. Rev. Lett. **100**, 034501 (2008).